Energy 290 (2024) 130278

Contents lists available at ScienceDirect

Energy

journal homepage: www.elsevier.com/locate/energy

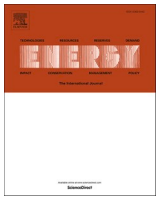

Thermodynamic analysis of small-scale polygeneration systems producing natural gas, electricity, heat, and carbon dioxide from biomass

Elie Antar *, Etienne Robert

Department of Mechanical Engineering, Polytechnique Montréal, Montréal, Québec, H3T 1J4, Canada

ARTICLE INFO

Handling Editor: Krzysztof (K.J.) Ptasinski

Keywords:
Polygeneration systems
Biomass gasification
Synthetic natural gas
Reversible fuel cells

ABSTRACT

Agricultural greenhouses are still heavily dependent on fossil fuel-based products despite the abundant residual biomass at their disposal. This paper presents two novel decentralized systems that can convert biomass simultaneously into synthetic natural gas (SNG), electricity, useful heat, and a CO_2-rich stream. To do so, the electricity and H_2/O_2 production features of reversible solid oxide cells (RSOCs) are exploited. A steam dual fluidized bed (DFB) gasifier is used in the first proposed system, while the second one adopts a simpler oxygen/steam-blown downdraft gasification approach. Thermodynamic simulations using Aspen Plus software reveal that the total polygeneration process efficiency could reach 86.6%, with a CO_2 generation capacity exceeding 275g per kilogram of biomass input. If not used inside the greenhouse atmosphere to enhance crop growth, this high-purity CO_2 stream could be sequestered/liquefied to render the process carbon negative. The flexibility of the polygeneration systems is investigated through parametric analysis, where maximum SNG efficiencies that are on par with large-scale plants are obtained. The possibility of storing surplus electricity from intermittent sources as chemical energy in SNG is also highlighted.

1. Introduction

Lignocellulose is the most abundant type of biomass on earth [1]. It can be found in large quantities throughout agricultural areas under the form of wood chips, corn stover, wheat straw, etc. Today, the use of these residual biomasses in the agricultural sector, essentially woody feedstocks, is mostly limited to biomass boilers often to supply heat-intensive needs such as warming greenhouses [2]. These low-efficiency furnaces, compared to natural gas or propane alternatives, usually only satisfy part of the greenhouses heating loads. The outstanding thermal energy requirements, as well as other energy-intensive agricultural practices are still supplied from fossil fuels [3]. Decentralized biomass gasification systems could potentially bridge this gap, while diminishing the expenses and carbon footprint of agricultural greenhouses. This is because versatile biofuels can be generated by gasification-based systems, which are generally considered the most cost-effective, practical, and efficient approach for converting lignocellulosic biomass [4].

Synthetic natural gas (SNG) is an example of such biofuels, which could be used instead of gasoline and diesel for transportation or power generation in greenhouses [5]. Frequently operated at pressures lower than 10 bar [6], SNG reactors feeding on biomass-derived syngas can be considered safe to adopt in greenhouses, unlike other reactors such as methanol (MeOH) or dimethyl ether (DME) biofuels, which optimally operate at 50–80 bar [7,8]. Also, syngas conversion fraction to SNG is significantly higher than for other biofuels, often exceeding 90% [9]. This reduces the number and complexity of the crude SNG purifying equipment that must be incorporated in the system. Biomass conversion to SNG has been frequently studied in the literature using flowsheet simulations, where net biofuel efficiencies on the order of 70% (based on the LHV) have been attained [10–13], albeit scarcely in the context of greenhouse applications. Despite this, single-product systems producing only SNG from biomass usually struggle to compete economically with conventional natural gas [14]. This is especially the case for small-scale applications that use much less than 20 MW biomass thermal power [15].

However, promising economic prospects have been reported for these systems where other useful energy forms besides SNG are co-generated, and most importantly, properly harnessed. For instance, relative to a standalone SNG system, Arteaga-Pérez et al. [16] attained a 12.7% reduction in SNG production cost simply by adopting an integrated plant topology where the heat that is co-generated in abundance

* Corresponding author.
E-mail address: elie.antar@polymtl.ca (E. Antar).

https://doi.org/10.1016/j.energy.2024.130278
Received 28 June 2023; Received in revised form 4 December 2023; Accepted 4 January 2024
Available online 5 January 2024

during the exothermic SNG process is recovered. Unlike large-scale systems that are centralized, heat recovery could be readily adopted in small-scale SNG systems decentralized in greenhouses since they require large amounts of local heating for most of the year, especially in northern climates. The requirement for heat recovery to improve the economics of small-scale SNG systems was also emphasized in other works [17,18], where authors also discussed how profitability can be increased by adopting multi-product systems when possible. The polygeneration concept is highly compatible with the energy landscape of agricultural greenhouses, since electricity and high-purity carbon dioxide are also needed, in addition to fuel and heating. Carbon dioxide is usually purchased and injected into the greenhouse atmospheres since its concentration in ambient air is suboptimal for crop growth, being particularly low during daytime around 150 ppm [19] relative to the optimal 700–1000 ppm concentration [20]. Despite these facts, polygeneration systems that can simultaneously produce SNG, electricity, heat and high-purity CO_2 from biomass have never been previously investigated, to the authors' knowledge.

In the literature, the polygeneration concept has generally received less attention than single-product or co-generation (biofuel or electricity and heat) systems, and is usually not discussed in the context of agricultural greenhouses. For instance, Clausen et al. [21] modelled two 5-MW tri-generation systems converting wood chips into either MeOH or DME, electricity, and heat, at a total efficiency between 87 and 88% (based on the LHV). Jana and De [22] proposed a 4-MW polygeneration plant, which converts agricultural waste to electricity, cooling, heating, and ethanol for rural areas. Techno-economic modelling demonstrated how the inherent flexibility of the polygeneration system and its synergy with the local utility needs contributed to profitability. However, in both of these studies, the biofuel reactors had to be operated at elevated pressures that exceeded 90 bar, as alcohols were produced, which could raise safety concerns in small-scale applications such as agricultural greenhouses. Heyne et al. [23] integrated an SNG biomass system with a steam power cycle for tri-generation of SNG, electricity, and district heat. Simulations predicted an SNG efficiency of 69.4% (based on the LHV), but the production of high-purity carbon dioxide was not considered, similar to the aforementioned studies. These research needs motivated our recent work [24], where two versions of a four-product polygeneration system were designed to meet the inputs required in agricultural greenhouses. Despite the 85% process efficiency, the biofuel yield had to be limited to only 14%, since MeOH was produced at relatively low sub-optimal pressures for safety considerations. We alleviate this compromise in the current study by considering SNG biofuel, which requires less severe conditions for optimal yield, and which could be readily handled or traded by greenhouses using existing natural gas distribution infrastructure.

Therefore, the goal of this study is to present and characterize the thermodynamic performance of novel polygeneration systems that are capable of converting biomass to synthetic natural gas, electricity, heat, and carbon dioxide. These products are highly demanded in agricultural greenhouses, and their simultaneous production efficiencies from biomass remain unknown. First, the designs of the two proposed systems are presented, essentially differing in the gasification stage, with steam dual fluidized bed and oxygen/steam-blown downdraft gasifiers considered. A description of the flowsheet modelling approach is then given, followed by the results. Here, the energy flow in each system is detailed, and parametric analysis is shown to highlight the features of each system and their flexibility to accommodate changes in energy demand.

2. Systems description

In this section, the layouts of both proposed systems are discussed, and the design choices for each stage in the biomass conversion process are justified. This is followed by the modelling approach used. The selected feedstock for this study is wood chips, which are widely available in agricultural settings and are a common choice for thermodynamic biomass conversion studies. Their ultimate and proximate analyses are shown in Table 1.

2.1. Drying and gasification

The first system proposed uses a steam dual fluidized bed gasifier (DFB) operating at atmospheric pressure as shown in Fig. 1. The DFB gasifier was developed by Vienna University of Technology, and is sometimes referred to as fast internally circulating fluidized bed (FICFB). It has been implemented in small-scale configurations rated at a few hundred kilowatts and large-scale multi-megawatts plants [25]. The syngas produced has high CH_4 and H_2 content, which renders steam DFB gasifiers a common choice for SNG production [12]. The process is allothermal, whereby the biomass is gasified by steam in a separate bubbling fluidized bed, and the residual char and bed material is transferred via an inclined chute to a fast circulating fluidized bed, where an oxidant is injected for combustion. The resulting gases are cleared from solid particles in a cyclone where the hot bed material is returned, via a loop seal, to the gasification chamber operating at 850°C to provide the required heat for the endothermic process. The chute and loop seal are fluidized by steam, and this prevents gas leakage from the combustion zone, providing almost N_2-free syngas, which is crucial for methanation reactors, even if air is used as an oxidant in the combustion chamber. The steam required for gasification is generated at 450°C, by using the system's excess heat, at a steam to biomass ratio (mass-based) of S/B = 1.5. DFB gasifiers typically operate in the range of S/B = 0.5–2.0 [25], where higher S/B ratios result in higher H_2/CO ratios in syngas, but lower cold gas efficiencies due to the incorporation of more steam. We opted to operate at the upper S/B range as increasing the H_2 content in syngas plays a key factor in enhancing the SNG yield, as shown later.

Before being fed to the gasifier, the biomass moisture content is reduced to 10% in a steam dryer that harnesses part of the heat generated by the other exothermic components of the system. Lowering the feedstock moisture level ensures adequate fluidization in the gasifier, as for a given S/B, which incorporates the water content in the biomass, the amount of fluidizing steam that is injected into the gasifier decreases with increasing biomass moisture. Instead of being vented, the generated steam from the dryer is recycled into the solid oxide electrolysis cell (SOEC), which plays a crucial role in the CO_2, SNG, and electricity generation stages as discussed later. This energy-efficiency measure of coupling a steam dryer to a SOEC has been previously discussed and used by Clausen [26] for the conversion of very wet biomass.

The second system proposed in this study adopts a downdraft gasifier as shown in Fig. 2. This is a simpler gasification approach that can be readily implemented in small and medium-scale systems rated between 10 kW and 10 MW [27]. Prior to gasification, the biomass is dried to 10% moisture in a steam dryer configuration similar to that described above. Within the gasifier, the biomass is first further dried, then

Table 1
Characteristics of wood chips [24].

Ultimate analysis (wt% dry basis)	
C	50.6
H	6.5
N	0.2
O	41.9
S	0.05
Cl	0.03
Proximate analysis (wt% dry basis)	
Moisture	45
FC	19.2
VM	80.1
Ash	0.7
LHV (MJ/kg wet basis)	12.1
HHV (MJ/kg wet basis)	14

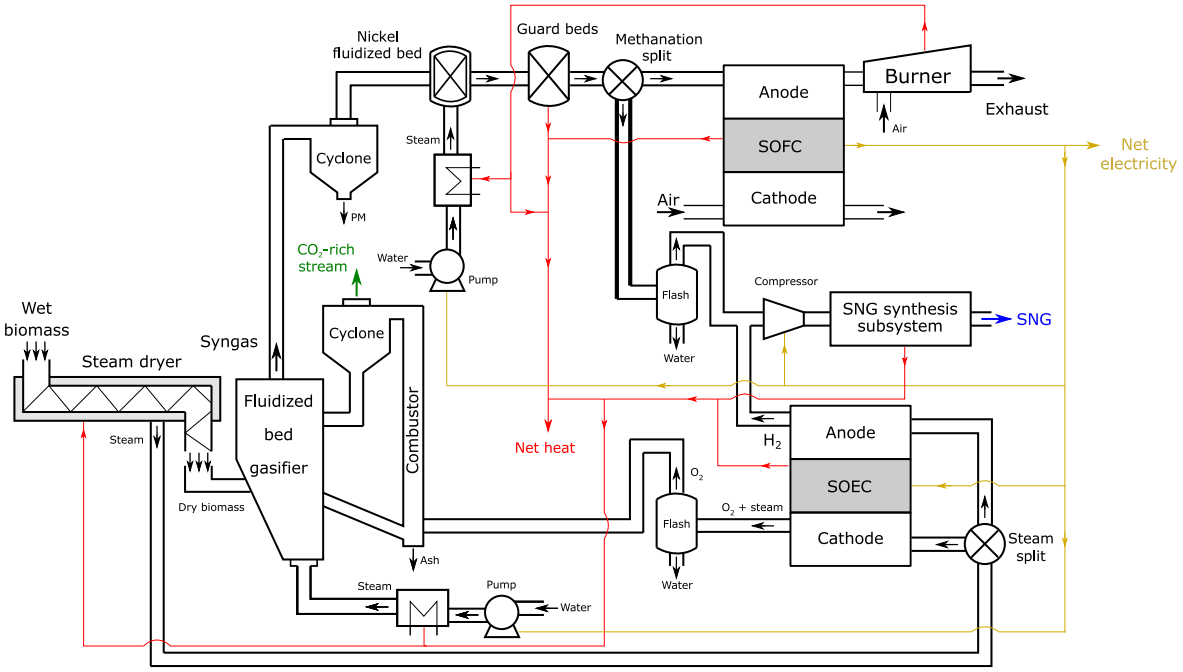

Fig. 1. Schematic representation of the dual fluidized bed gasifier-based SNG system.

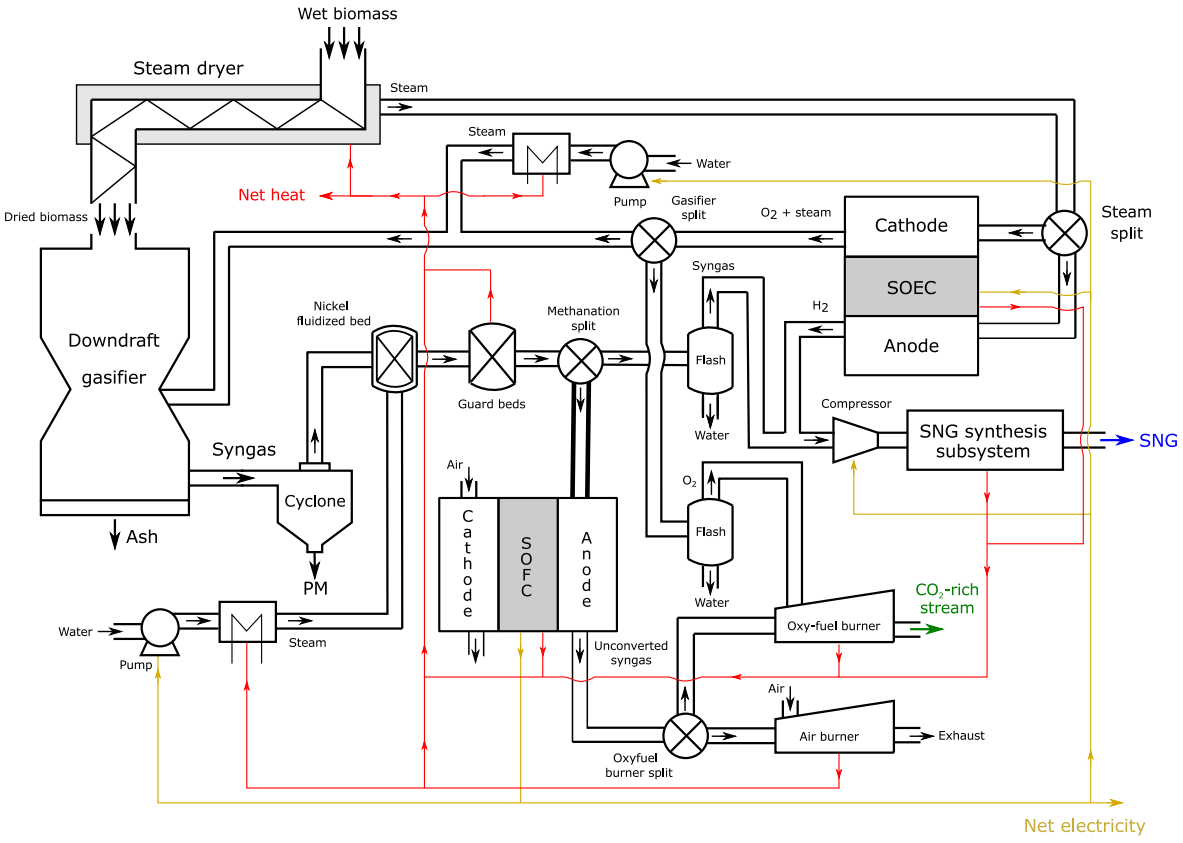

Fig. 2. Schematic representation of the downdraft gasifier-based SNG system.

pyrolyzed, oxidized, and finally reduced. The flow of solid and gaseous products is co-current, leading to higher gas exit temperatures compared to updraft gasifiers, and consequently less tar in the syngas. A steam-oxygen mixture is used as a gasification agent, which yields N_2-free syngas with elevated H_2 content, as required by the methanation reactor. A SOEC produces this steam-oxygen mixture at an equivalence ratio (ER) of 0.2. The ER is defined as the ratio of the actual over the required O_2 flow rate needed to achieve stoichiometric combustion for a given amount of biomass. A steam to biomass ratio of S/B = 1.5 is ensured by generating steam using excess heat from other exothermic

components, as the sweeping steam from the SOEC cathode is not enough.

2.2. Syngas cleaning

To clear the generated syngas from undesired contaminates that could poison/deactivate catalysts and clog downstream equipment, hot gas cleaning techniques are adopted in both systems following gasification. These are attractive for small-scale applications as only limited waste handling is required, and as less thermal energy is lost since the syngas must not be cooled to low temperatures [28]. As seen from Figs. 1 and 2, a cyclone is first used to clear the solid particulate matter (PM) entrained in syngas such as char, ash, soot, dust, etc. Then, a steam fluidized nickel bed operating at 780°C with a steam to carbon ratio S/C of 3 is used for tar abatement. Nickel-based catalysts at this temperature and steam content have been shown to yield very high tar conversion efficiencies (>99% [29]). The required steam is generated from the combustion of unconverted syngas left over at the end of the biomass conversion process.

For the systems to accommodate different agricultural feedstock containing higher sulfur content than wood chips, Sato and Fujimoto [30] proposed doping the nickel-based catalyst with WO_3 to avoid sulfur poisoning. During their 100-h test, the authors have shown that their Ni-WO_3/MgO–CaO catalyst tar conversion fraction remains above 95% even when the H_2S content in syngas is as high as 400 ppm. It should be noted that the H_2S content of syngas is typically on the order of 100 ppm for most biomass feedstock [31]. Following tar conversion, acid gas species such as H_2S and HCl are removed in two in-series ZnO and activated carbon guard beds operating at 400°C [21,32].

2.3. Electricity production

In both systems, the methanation split component shown in Figs. 1 and 2 sends part of the cleaned syngas stream for methane synthesis as discussed next, and the other part to an 850°C solid oxide fuel cell (SOFC) for electricity generation. The splitting fraction is variable and offers the flexibility of increasing the fraction of desirable energy forms over others, as demonstrated in the results section. Part of the electricity generated is used to power the SOEC and other auxiliary components of the system, with the remaining quantity available for powering the greenhouse. Various experimental studies reporting the successful operation of SOFCs with biomass-derived syngas can be found in the literature [33–35]. A handful of reasons motivate the use of a SOFC in this study, the first being its ability to generate electricity more efficiently and with very low pollutant emissions compared to conventional heat engines [36]. Upon replacing a micro gas turbine with a SOFC, Minutillo et al. [37] realized a 7.3% increase in efficiency for their combined heat and power biomass conversion system. The versatility of SOFCs is also highly compatible with the polygeneration characteristics desired in agricultural greenhouses. It is an exothermic component that co-produces heat at high temperatures, which can be either used internally in the system where needed or supplied to the greenhouse. It is also known for its reversibility, or its ability to operate as a SOEC. When fed with electricity and water, two separate streams of H_2 and O_2 are produced. The former is needed for the methanation stage as shown next, while the latter is crucial for the gasification stage, and as discussed in section 2.5, for the production of high-purity CO_2 needed in the greenhouse.

2.4. Methanation

Methane is synthesized from syngas according to the CO methanation and water gas shift (WGS) reactions [5]:

$$CO + 3H_2 \leftrightarrow CH_4 + H_2O \quad (1)$$

$$CO + H_2O \leftrightarrow CO_2 + H_2 \quad (2)$$

The yield is highly dependent on the syngas composition, where a linear combination of reactions 1 and 2 reveals the optimal feed gas module (M) [38]:

$$M = ([H_2] - [CO_2]) / ([CO] + [CO_2]) = 3 \quad (3)$$

with the terms in the square brackets being the molar quantities of the species in the feed stream. As shown in the results section, the syngas module after the gas cleaning stage in both systems is significantly less than three. Nonetheless, the incorporation of SOECs averts suboptimal syngas conversion to CH_4, whereby the co-generated H_2 is used to enrich the dried syngas stream and render its module optimal at M = 3. The conditioned mixture is then compressed to 10 bar and fed into the "SNG synthesis subsystem" shown in Figs. 1 and 2. Here, syngas is cooled and injected into a fixed bed nickel catalytic reactor at 270°C [12]. The exothermic reactor is cooled with water, and the generated steam can be used to heat the greenhouse. Water from the outlet stream of the reactor is condensed in a 40°C flash separator, before purifying the crude SNG stream in a pressure swing adsorption unit (PSA) [10].

2.5. Heat and carbon dioxide generation

Following the previous discussion, one can see that several components producing useful heat for greenhouses are already incorporated throughout the biomass conversion process. The final source is found following the electricity generation stage, where the unconverted syngas leftover from the SOFC is burned. Part of the heat is used for generating the steam needed in the tar abatement reactor, and the remaining recoverable quantity is for the greenhouse.

To produce the carbon dioxide required for greenhouse atmosphere enrichment, oxygen from the SOEC is used instead of air in the DFB gasifier combustion chamber, whose sole purpose usually is to produce the heat required for gasification. Heidenreich and Foscolo [28] are one of the few authors to discuss this opportunity with DFB gasifiers, albeit briefly, in their review paper. For the downdraft gasifier-based system, a fraction of the leftover syngas from the SOFC is combusted in an oxyfuel burner as shown in Fig. 2. The required oxygen is generated by the SOEC such that a lean equivalence ratio ER = 1.2 is maintained, in addition to the oxygen required for gasification. In both systems, the resulting exhaust stream is of high purity, containing more than 92% CO_2 with the remaining quantity being essentially O_2. If not used in the greenhouse, these high-purity CO_2 streams could be sequestrated or liquefied, potentially rendering the biomass conversion process carbon negative.

2.6. Modelling and operating conditions

The Aspen Plus flow sheet simulator, which performs rigorous energy and mass balance calculations, is used to predict the performance of the biomass conversion systems described above. The software is convenient for the simulation of systems with many components, as it can be readily configured to simultaneously meet multiple related design specifications, such as the SOEC oxygen production rate, gasifier equivalence ratio, and net electricity production. Also, the effect of varying the operating conditions can be conveniently studied by the embedded sensitivity analysis feature. A thermodynamics-based modelling approach is implemented, which is a common choice when analyzing the energy feasibility of novel systems and identifying desirable operating conditions. This is because results can be generalized, and are independent of the reactors design, unlike kinetic rate models that are also more computationally intensive [11].

Similar to related previous work [39,40], the Peng-Robinson cubic equation of state is used for gas phase processes, while the STEAM-TA equation embedded in Aspen Plus is used for steam. Steady state is assumed along with negligible pressure losses across system

components, and tar in crude syngas is modelled as 60% benzene (C_6H_6), 20% toluene (C_7H_8), and 20% naphthalene ($C_{10}H_8$) by weight [41]. Experimentally-validated models are used for the different system components such as the gasifier, tar reformer, and methanation reactor. These models are summarized in Table 2, and for more details on the user-defined subroutines, readers are kindly referred to our earlier work [24], where similar components were adopted, albeit in a different plant layout. Table 2 also includes a list of the typical process design parameters such as biomass moisture downstream of the dryer, gasifier equivalence and steam to biomass ratios, tar abatement reactor steam to carbon ratio, methanation reactor pressure and temperature, and the temperatures and current densities (i) of the reversible solid oxide cells (RSOCs).

The constant area specific resistance (ASR) approach is used to model the SOFC and SOEC. Consequently, the operating voltage (V_{op}) of the cells is computed as:

$$V_{op} = V_{rev} - iASR \tag{4}$$

with V_{rev} being the Nernst or reversible voltage for the given operating conditions, and i the current density (A/m^2, positive for the SOFC and negative for the SOEC) computed as follows [46]:

$$V_{rev} = V^o - \frac{\Delta\hat{s}}{nF}(T - T_o) - \frac{RT}{nF} ln\left(\frac{\prod a_{products}^{v_i}}{\prod a_{reactants}^{v_i}}\right) \tag{5}$$

Table 2
Summary of the Aspen Plus models used for each component in the systems. Detailed description can be found in Antar and Robert [24].

Components	Model	Operating conditions
Steam dryer	RStoic reactor	T_{steam} = 200°C, P = 1 bar, $T_{biomass}$ = 120°C, 10% moisture level
Steam blower and pumps	Compr pressure changer	$\eta_{isentropic}$ = 80%, $P_{increase}$ = 0.05 bar
Dual fluidized bed gasifier	Doherty et al. [42]	T = 850°C, P = 1 bar, S/B = 1.5, $ER_{combustion,\ chamber}$ = 1.2, tar = 9.5 g/Nm^3, heat loss = 5.5% of biomass HHV
Downdraft gasifier	Han et al. [43]	T = 775°C, P = 1 bar, ER = 0.2, S/B = 1.5, tar = 5 g/Nm^3, heat loss = 5.5% of biomass HHV,
Cyclones	SSplit splitters	T_{loss} = 100°C, char and ash split fraction = 1
Tar reformer	RStoic + RGibbs reactors [11]	S/C = 3, T = 780°C, conversion fraction = 1
Guard beds	Sep separator	T = 400°C, T_{loss} = 100°C, acid gas split fraction = 1
Flash condensers	Flash2 separator	T = 40°C, duty = 0
Compressors	Compr pressure changer	$\eta_{isentropic}$ = 80%, $P_{increase}$ = 10 bar
Methanation reactor	RGibbs reactor [44]	T = 270°C, P = 10 bar, PSA split fraction = 0.98
SOFC	Constant area specific resistance (ASR) [24, 45]	T = 850°C, P = 1 bar, $U_f = U_o$ = 0.7, ASR = 0.2 Ω.cm^2, i = 0.5 A/cm^2 when the methanation reactor split fraction is zero, with recuperative heat exchangers, T_{loss} = 100°C
SOEC	Constant ASR [24,45]	T = 850°C, P = 1 bar, U_o = 0.7, ASR = 0.2 Ω.cm^2, $V_{op} = 1.3 > V_{thermoneutral} = 1.29$V, with recuperative heat exchangers, T_{loss} = 100°C
Leftover syngas burners	RGibbs reactor	ER = 1.2, P = 1 bar, $\eta_{combustion}$ = 85%
Heat exchangers	Heater and HeatX Exchangers	ΔT_{min} = 15°C (gas-liquid) and 30°C (gas-gas)

$$V^o = -\frac{\Delta\hat{g}^o}{nF} \tag{6}$$

$$i = \frac{I}{A} = \frac{n_{H_2,r}(nF)}{A} \tag{7}$$

$\Delta\hat{s}$ and $\Delta\hat{g}^o$ are the molar-specific changes in entropy and Gibbs free energy, respectively, across the SOFC/SOEC, V^o is the reversible voltage at standard conditions, and the last two terms in equation (5) account for the effect of temperature, pressure and activity. The average molar composition of the reactants and products are used for determining the activity of species in the products or reactants streams $a_{products}^{v_i}$ and $a_{reactants}^{v_i}$. In equation (7), $n_{H_2,r}$ is the number of H_2 moles undergoing electrochemical reactions, as determined by an equilibrium (RGIBBS) reactor for the syngas-fed SOFC. For the steam-fed SOEC, the H_2O utilization factor is 0.7. The airflow entering the SOFC cathode is such that a fuel utilization factor of U_f = 0.7 is maintained. This contant area specific resistance approach is extensively used in similar thermodynamic system studies involving high-temeprature reversible fuel cells operating at mid-range current densities 0.5–1 A/cm^2 and ASR 0.2–0.25 Ω-cm^2 [45,47,48]. The results from these papers have been validated against experimental data, and were succesfully replicated as initial test cases in this study.

The power outputs of the simulations are made non-dimensional using the thermal power of the biomass input, based on its HHV (500 kW):

$$\eta_{ele} = P_{net} \,/\, (\dot{m}HHV)_{BM} \tag{8}$$

$$\eta_{th} = \dot{Q}_{net} \,/\, (\dot{m}HHV)_{BM} \tag{9}$$

$$\eta_{biofuel} = (\dot{m}HHV)_{biofuel} \,/\, (\dot{m}HHV)_{BM} \tag{10}$$

$$\eta_{tot} = \eta_{ele} + \eta_{th} + \eta_{biofuel} \tag{11}$$

P_{net} (Eq. (8)) is the net electrical power produced from the SOFC, after powering the auxiliary components, and similarly $\dot{Q}_{net}$ (Eq. (9)) is the neat heat produced after supplying the endothermic processes of the systems. $\dot{m}$ (Eqs. (8)–(10)) is the mass flow rate of the wet biomass (BM) used or the biofuel produced which could be either SNG or unrecycled H_2. The goal is to keep the values of the four efficiencies (Eqs. (8)–(11)) positive, and not rely on external energy inputs in addition to biomass.

3. Results

3.1. Dual fluidized bed gasifier-based SNG system

For a clear demonstration of the energy flow in the dual fluidized bed gasifier-based system, its Sankey diagram is shown in Fig. 3. The energy of each stream is normalized with the thermal energy of the input biomass. 7.5 out of the 9% of the total energy used in the drying stage is recovered as steam. Char with 6% energy content is expended in the combustion chamber of the DFB gasifier, which supplies 5.5% heat to the gasification chamber. Steam with 15% energy content generated from the system's residual heat is injected into the gasifier, leading to a cold gas efficiency of η_{CG} = 88.9%. Energy losses at 8.4% are sustained during the gas cleaning stage, after which 25% of the generated syngas is sent for methanation and 75% to the SOFC. This is only a particular case for demonstration, and the effect of varying the methanation split fraction on SNG and other yields is discussed in detail later in this section.

Recuperative heat exchangers are used in the SOFC to heat the input streams from 300 to 850°C, where 25.9% of the total input energy is obtained as electricity. The efficiency of the SOFC based on the first law of thermodynamics is $\eta_{I,SOFC}$ = 41.8%. However, considering the maximum reversible power for the amount of syngas undergoing elec-

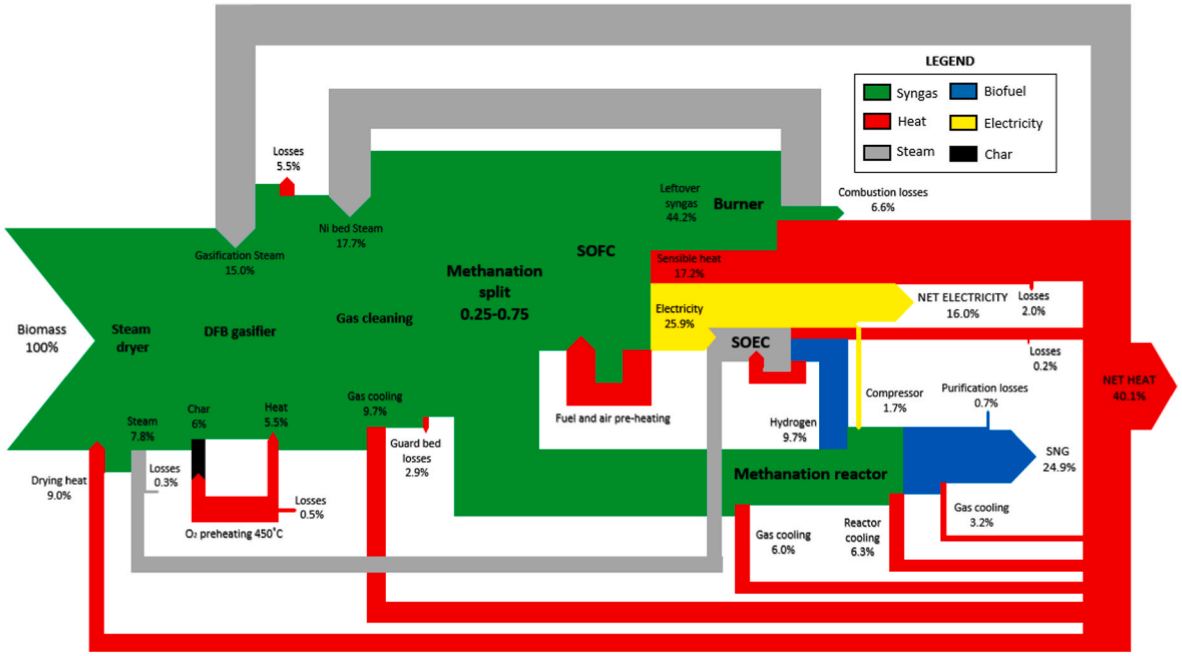

Fig. 3. Sankey diagram of the dual fluidized bed gasifier-based SNG system. The energy of the streams is normalized with the thermal energy of the biomass input (based on the HHV).

trochemical reactions, a decent second law efficiency of $\eta_{II,SOFC} = \eta_{I,SOFC}/\eta_{SOFC,reversible} = P_{ele,prod}/\dot{m}\Delta g = 91.3\%$ is revealed, where $P_{ele,prod}$ is the amount of electricity produced by the SOFC as calculated by the constant ASR (Table 2). After feeding the SOEC with 8.2% of the total energy as electricity and powering the other auxiliary components, the net electrical efficiency of the system is $\eta_{ele} = 16.0\%$.

The SOEC yields 9.7% of the total energy as H_2 at a relatively low efficiency of $\eta_{II,SOEC} = \dot{m}\Delta g/P_{ele,consumed} = V_{rev}/V_{op} = 66\%$, since to benefit from simple heat management it has to be exothermic, and hence be operated at or above its thermoneutral voltage of 1.29 V, a considerably larger value than the Nernst or reversible voltage $V_{rev} = 0.85$ V. The operating voltage of the SOEC is calculated using the constant ASR model referenced in Table 2, and described in detail in earlier works [24,45]. The generated H_2 enriches the syngas before being fed into the methanation reactor, which produces SNG at $\eta_{SNG} = 24.9\%$ and an abundance of heat. Summing the total amount of recoverable thermal energy in the system reveals a $\eta_{th} = 40.1\%$, contributing to a total polygeneration process efficiency of $\eta_{tot} = 81.0\%$. On top of this, 96g of CO_2 is generated for the greenhouse atmosphere per kilogram of 45%-wet biomass input. If desired, this can be considerably increased at the expense of electricity as discussed later.

Fig. 4 highlights the flexibility of the proposed polygeneration system by showing the effect of varying the fraction of syngas sent to the methanation reactor (R_{meth}) on the different outputs. This is controlled

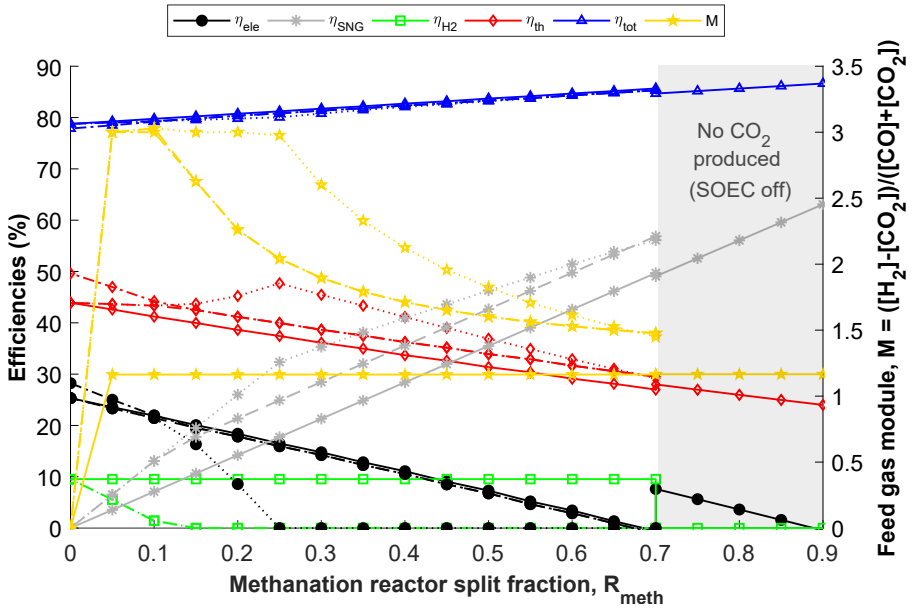

Fig. 4. Variation in the output of the dual fluidized bed gasifier-based SNG system as a function of the fraction of syngas sent to the methanation reactor. Four hydrogen recycling modes are considered: 0 (——), 1 (– – –), 2 (— – —), and 3 (.....).

by the methanation split component shown earlier in Fig. 1. Various H_2 recycling modes are considered as described in Table 3. For the extreme case of $R_{meth} = 0$, no SNG is produced in all modes, and electricity and heat output are $\eta_{ele} = 25.3\%$ and $\eta_{th} = 43.9\%$, respectively for mode 1. A net quantity of H_2 is also produced at $\eta_{H_2} = 9.5\%$ as none of it can be recycled into the SNG reactor. Nonetheless, this H_2 can be recycled into the SOFC to maximize electricity output to $\eta_{ele} = 28.2\%$ if desired (mode 2). On the other side, the maximum attainable split fraction while simultaneously producing CO_2 is $R_{meth} = 0.7$, yielding $\eta_{SNG} = 53.9\%$. If CO_2 production is sacrificed by turning off the SOEC and using air in the combustion chamber of the gasifier, $R_{meth} = 0.9$ can be achieved, yielding a maximum $\eta_{SNG} = 63.1\%$ (shaded region Fig. 4). Here, no net quantity of electricity is produced, and net heat production drops to $\eta_{th} = 24\%$, since the quantity of leftover syngas from the SOFC sent to the burner decreases. Consequently, this enhances the total system efficiency, which goes from $\eta_{tot} = 78.7\%$ at $R_{meth} = 0$ to $\eta_{tot} = 86.2\%$ at $R_{meth} = 0.9$ as the exhaust losses from the burner are minimized.

The prominent role played by the SOEC in the SNG production process is highlighted by considering mode 0 in Fig. 4. It can be seen that if H_2 enrichment is not adopted at $R_{meth} > 0$, the feed gas of the methanation reactor is always significantly deprived of H_2, with a module of M = 1.16. This clearly limits the SNG yield, which at $R_{meth} = 0.1$ for example is $\eta_{SNG} = 7.1\%$, but which almost doubles to $\eta_{SNG} = 13.7\%$ upon making M = 3 as H_2 from the SOEC is used (modes 1 and 2). As the split fraction is increased, the H_2 co-produced by the SOEC as it supplies the combustion chamber of the gasifier with O_2 eventually becomes insufficient to attain M = 3. For instance, at $R_{meth} = 0.2$, M = 2.3 even when all the produced H_2 is recycled, resulting in only $\eta_{SNG} = 21.3\%$. If more SNG is desired, part of the net electricity produced by the system $\eta_{ele} = 17.8\%$ can be diverted to the SOEC to produce more H_2 and render M = 3 (mode 3). Upon doing so, SNG yield increases to $\eta_{SNG} = 26.0\%$, and excess O_2 is produced, which can be used to increase CO_2 production in the oxyfuel burner, as discussed later. As the split fraction is further increased, the entire system's net electricity becomes insufficient to increase the module of the feed gas to M = 3. At $R_{meth} = 0.3$, the maximum feed gas module that can be attained is M = 2.60, when all the excess electricity from the SOFC is used. The SNG yield at $\eta_{SNG} = 28.5\%$ is still higher than that attained at lower R_{meth} where M = 3, but now electricity from an external source, if available, could be injected into the SOEC and get stored as chemical energy in SNG. This concept has been previously investigated on a large scale in the context of flexible energy utilization and storage from intermittent sources such as wind, where bio-SNG is generated from electrolytic H_2 when the prices of electricity are low [17].

Fig. 5 presents the resulting changes in efficiencies when electricity is injected into the biomass conversion system at $R_{meth} \geq 0.3$, after using all the power generated from the SOFC (mode 3). Strictly speaking, the conversion fraction of electricity to SNG is dependent on R_{meth} and the amount of electricity to be stored. This is because both of these parameters affect the efficiency of the SOEC, which decreases at smaller R_{meth} and larger electricity input, since the SOEC overpotential is higher. Nonetheless, the implications on SNG yield are negligible at power inputs lower than 10%, and from the slopes of the efficiency lines which are highly linear under these conditions, it is revealed that the system is able to convert roughly 40% of input electricity into SNG, with the remaining 55% to heat, and 5% to unrecoverable losses. Also, for every kilogram of biomass input, injecting an additional 1% electricity into the system contributes to the production of 23g of CO_2. From a thermodynamics point of view, the maximum amount of electricity that can be stored by the system in SNG for given biomass input is only limited by the syngas module not exceeding M = 3. Otherwise, the H_2 conversion fraction to CH_4 and consequently the total efficiency of the process would deteriorate. Since the feed gas module decreases with R_{meth}, higher split fractions could in theory offer larger storing capacities. At $R_{meth} = 0.5$ for instance, the maximum amount of electricity that can be stored in SNG is equivalent to 60% of the input biomass energy. This is more than double the maximum energy that can be stored at $R_{meth} = 0.35$. However, injecting this amount of electricity into the SOEC results in a drastic current density increase, $\Delta i_{SOEC} = 5.8$ A/cm^2 in this case. This is likely to be outside the practical operating range, which requires SOEC-specific kinetic rate attributes to be accurately determined.

Table 3
Description of the different H_2 recycling modes adopted in this study.

Mode	Description
0	None of the H_2 co-produced by the SOEC as it feeds the gasifier with O_2 is recycled into the system.
1	The produced H_2 is recycled into the methanation reactor to optimize the feed gas module when $R_{meth} > 0$, and any excess is extracted from the system.
2	The excess H_2 from mode 1 is recycled into the SOFC.
3	All net generated electricity is fed into the SOEC to maximize H_2 enrichment when needed. Excess O_2 is produced.

The high-purity carbon dioxide generation rate of the system can be increased by burning part of the leftover syngas from the SOFC in an oxyfuel burner, similar to the downdraft gasifier-based configuration. This comes at the expense of the electrical power output since more O_2 must be generated by the SOEC. Fig. 6 shows the efficiencies as a function of the enhanced CO_2 generation rate at different R_{meth}, when the system is operating under mode 0. The SNG and total efficiencies are not included since they are essentially invariable with the amount of CO_2 produced. The SOEC is mainly responsible for the increased heat generation at higher CO_2 levels, due to its larger overpotential and therefore lower efficiency when more electricity is fed to it. This also explains the parabolic behavior of the system's electrical efficiency curves, where it can be seen that more electricity is consumed per kilogram of CO_2 at higher generation rates for all R_{meth}. For instance, below 0.2 $kg_{CO2}/kg_{Biomass.wet}$, electrical output drops on average by 4.6% for every 100g of CO_2 generated per kilogram of wet biomass input. However, between 0.3 and 0.5 $kg_{CO2}/kg_{Biomass}$, a larger amount of electricity at 6.8% is consumed for every 100g of CO_2 produced per kilogram wet biomass input. The maximum high-purity CO_2 generation capacity of the system that can be theoretically attained while only running on biomass occurs at $R_{meth} = 0$. Assuming that the SOEC can accommodate the resulting 3.5 A/cm^2 current density increase, a maximum of 529g of CO_2 can be generated per kilogram of wet biomass input. This represents a maximum potential carbon recovery rate of 52 mol per 100 mol of carbon input into the system ($n_{C,rec}/n_{C,in}$), as can be seen from Fig. 6. At this point, zero net electricity is generated, and H_2 production peaks at $\eta_{H_2} = 25.0\%$. In Fig. 6, Δi_{SOEC} is defined as the change in the current density of the electrolysis cell relative to the baseline operating condition where CO_2 is produced at 0.096 $kg_{CO_2}/kg_{biomass}$.

3.2. Downdraft gasifier-based SNG system

The energy flow in the downdraft gasifier-based system is shown in the Sankey diagram of Fig. 7. After the 10%-moisture drying stage, where a significant portion of the generated steam is recovered, the dried biomass is gasified at a cold gas efficiency of $\eta_{CG} = 76.4\%$. This is notably inferior to the efficiency of the DFB gasifier (88.9%), since the quantity of CO_2 that dilutes the generated syngas is 50% larger in the downdraft gasifier. Steam generated from the leftover syngas burner at a total energy of 18.6% is used for tar abatement in the gas cleaning stage, after which a particular methanation split of 0.1–0.9 is taken for illustration.

In the SOFC, 29.3% electricity is generated at $\eta_{II,SOFC} = 87.7\%$. However, a large fraction equivalent to 20.9% of the total input energy is directly injected into to the SOEC. This is considerably more than the 8.2% electricity required by the SOEC in the first system, since the downdraft gasifier requires double the amount of O_2 in the combustion chamber of the DFB gasifier, and since in addition to gasification, an

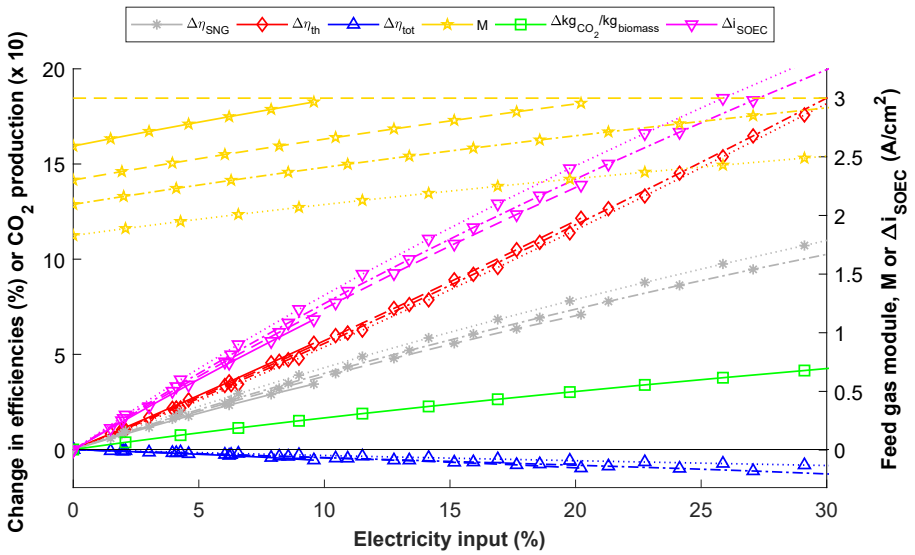

Fig. 5. Change in output when electricity from an external source is supplied to the system operating under mode 3. R_{meth} = 0.3 (——), 0.35 (– – –), 0.4 (— – –), and 0.5 (.....).

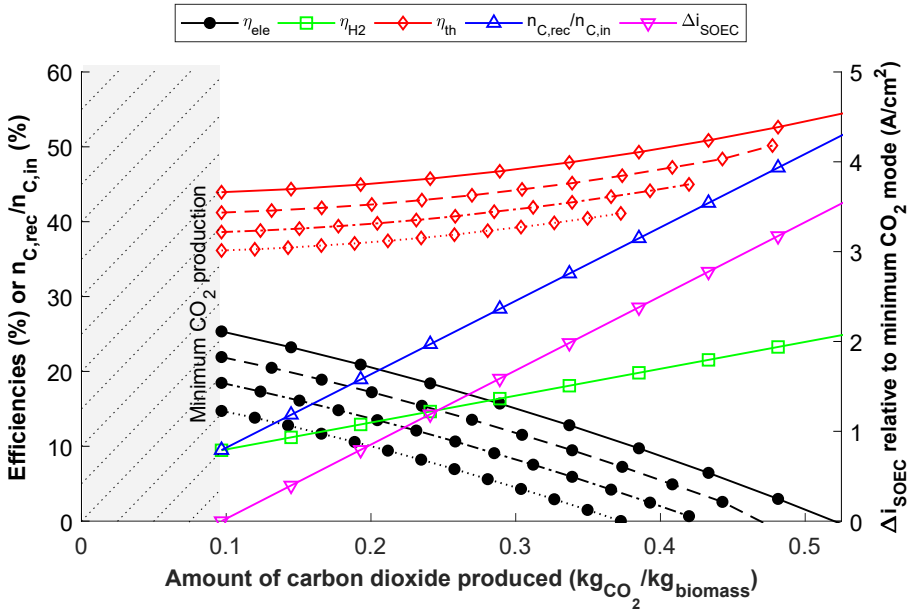

Fig. 6. Efficiencies at different CO_2 generation rates under R_{meth} = 0 (——), 0.1 (– – –), 0.2 (— – –), and 0.3 (.....). No H_2 is recycled into the system (mode 0).

oxyfuel burner must be used here for CO_2 production. After powering the other auxiliary components in the system such as compressors and pumps, a net electrical efficiency of η_{ele} = 7.4% is obtained. Leftover syngas from the SOFC is again split at 0.9–0.1 between the air and oxyfuel burners, which have total combustion losses of 9.1%. For this split fraction, 90g of CO_2 is generated by the oxyfuel burner per kilogram of wet-biomass input into the system. On the other hand, the SOEC generates 23.2% H_2, of which, 10.5% is fed to the methanation reactor to render the feed gas module optimal at M = 3, and 12.7% is recycled into the SOFC to enhance electricity generation. In the former, 13.7% SNG is synthesized, with the possibility of considerably increasing the yield by varying the methanation split fraction as shown next. Heat is produced by the system at η_{th} = 56.9%, leading to a total efficiency of η_{tot} = 78.0%, which can also be enhanced by increasing the methanation split fraction.

The effect of varying the methanation reactor split fraction on the output of the downdraft gasifier-based system is shown in Fig. 8. The trends are similar to the DFB gasifier-based system that was discussed in the previous section (Fig. 4), but the actual efficiencies are clearly different. For instance, the maximum electricity output for the downdraft gasifier-based system is η_{ele} = 16.7% at R_{meth} = 0 (mode 2). This is notably smaller than for the DFB gasifier-based system (η_{ele} = 28.3%), since more electricity is consumed by the SOEC here, as shown earlier. As a result, this reduces the maximum methanation reactor split fraction that could be attained, which is R_{meth} = 0.325 in this case (vs R_{meth} = 0.65 for the first system when the SOEC is operational), limiting the maximum SNG yield to η_{SNG} = 33.0% (vs η_{SNG} = 53.9% for the first system). It should be noted that since pure O_2 is crucial for the production of N_2-free syngas in downdraft gasifiers, not supplying electricity to the SOEC to attain higher R_{meth} is impossible. As shown earlier, this is not the case with the indirect gasification technology used in the first system, where a maximum R_{meth} = 0.9 and η_{SNG} = 63.1% can be

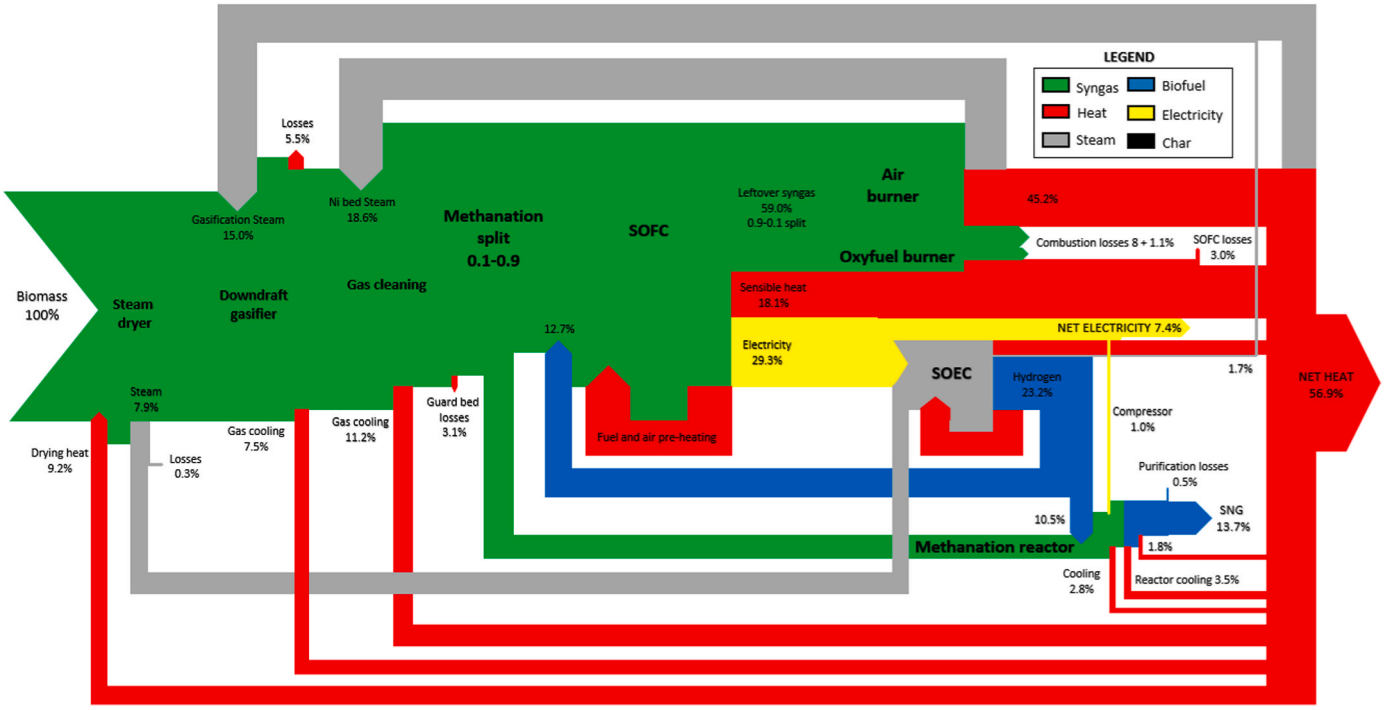

Fig. 7. Sankey diagram of the downdraft gasifier-based SNG system. The energy of the streams is normalized with the thermal energy of the biomass input.

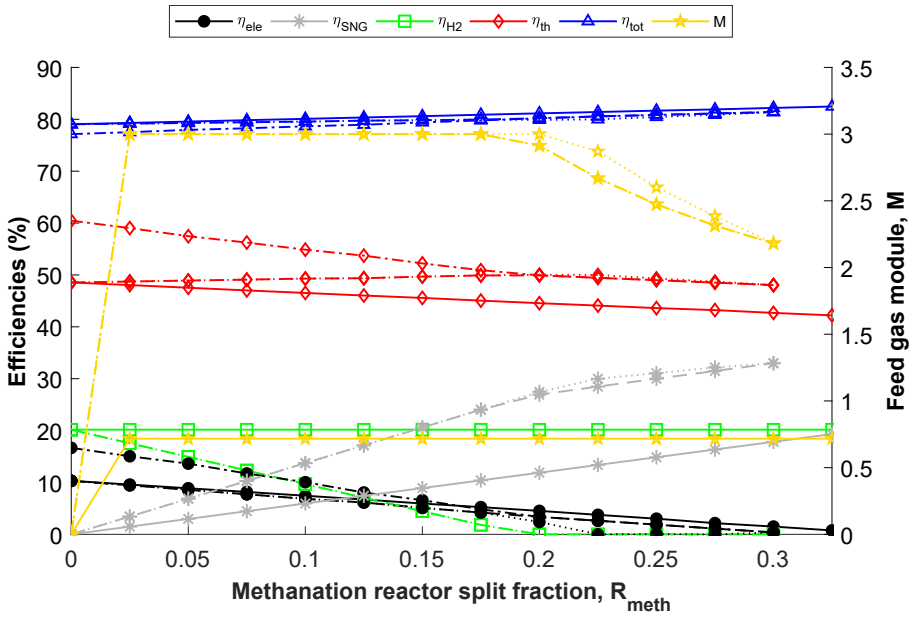

Fig. 8. Variation in the output of the downdraft gasifier-based SNG system as a function of the fraction of syngas sent to the methanation reactor. No leftover syngas from the SOFC is sent to the oxyfuel burner. Hydrogen recycling modes 0 (——), 1 (– – –), 2 ((— – –), and 3 (.....) are analyzed.

attained. Therefore, it can be said that adopting a simple downdraft gasification approach comes at a price of lower flexibility in energy output.

As discussed earlier, the fact that the feed gas module is less than M = 3 at larger split fractions, even when all the electricity generated by the SOFC is used for H_2 enrichment, means that this system also offers the additional feature of storing electricity in SNG if needed. Fig. 9 shows the resulting changes in efficiencies when electricity is injected into the SOEC of the downdraft gasifier-based system (at $R_{meth} = 0.4$), and compares its storage efficacy to that of the first system (at $R_{meth} = 0.5$). It can be seen that the electricity-to-SNG conversion efficiency of the downdraft gasifier-based system is higher than that of the first system. On average, 54% of the input electricity is converted to SNG, 40% to heat, and the remainder 6% is lost, for a given biomass input. The superior performance is attributed to the SOEC, whose current density is more than 1.5 times less sensitive to the amount of injected electricity when it comes to the downdraft gasifier-based system, as the electrode area of the SOEC here is twice as large as that of the first system. Consequently, this leads to a smaller increase in the operational voltage of the SOEC ($V_{op} \sim i$) in the downdraft gasifier-based system, and hence a smaller drop in $\eta_{II,SOEC}$ ($\sim V_{op}^{-1}$) as seen from Fig. 9. Given that the designs of the systems are not focused on electricity storage, which is in

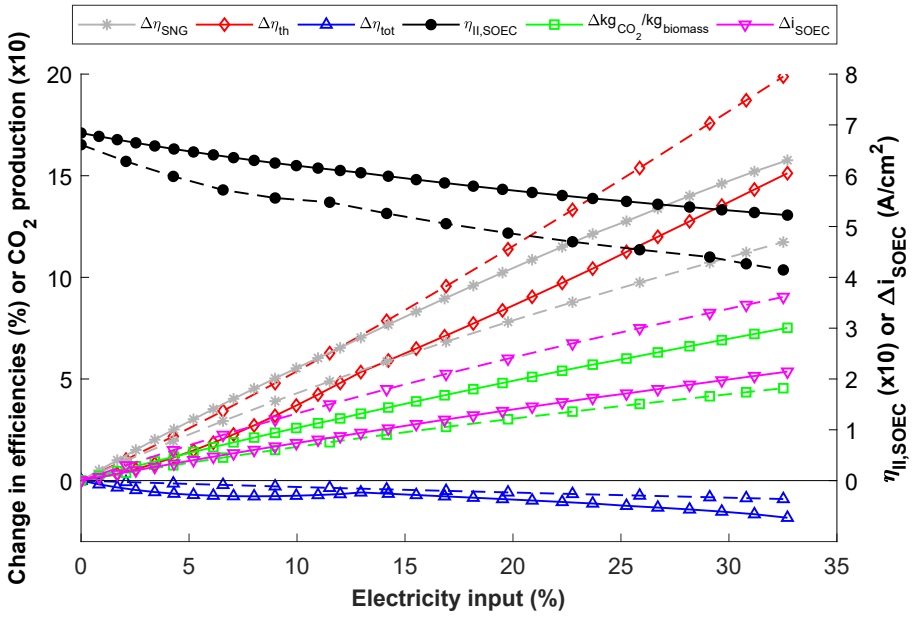

Fig. 9. Changes in efficiencies when electricity from an external source is injected into the downdraft gasifier-based system (——) and the DFB gasifier-based configuration (– – –) both operating in mode 3.

fact an additional feature due to the versatility of the proposed configurations, the storage efficiencies can be considered decent. This is in comparison to systems specifically designed for biomass conversion and electricity storage in SNG adopting conventional steam electrolysis which have an efficiency on the order of 70% [49].

In the downdraft gasifier-based system, O_2 must be supplied to the oxyfuel burner for the production of a high-purity CO_2 stream, in addition to the quantity needed for gasification. Fig. 10 presents the variation in efficiencies with the amount of CO_2 produced. The slopes of the trend lines being nearly constant in the range considered, it can be said that electricity production drops only by approximately 3.7% for every 100g of CO_2 generated per kilogram of biomass input. This is lower than the average electrical power consumed by the DFB gasifier system to produce the same quantity of CO_2, with its steeper electrical efficiency curve shown in Fig. 10. As discussed earlier, this is attributed to the superior SOEC performance whose current density sensitivity to CO_2 production is conveniently three times smaller. However, the maximum CO_2 quantity that can be generated per kilogram of biomass input in the downdraft gasifier-based system is only 275g at $R_{meth} = 0$ (vs 529g for the first system). This leads to a maximum carbon recovery rate of 27 mol per 100 mol of carbon input (vs 52 mol for the first system). H_2 production peaks here at $\eta_{H_2} = 28.1\%$.

3.3. System comparison and discussion

The efficiencies of the two proposed SNG polygeneration systems are summarized in Fig. 11 and Table 4, and compared with two MeOH-based four-product polygeneration plants introduced in previous work

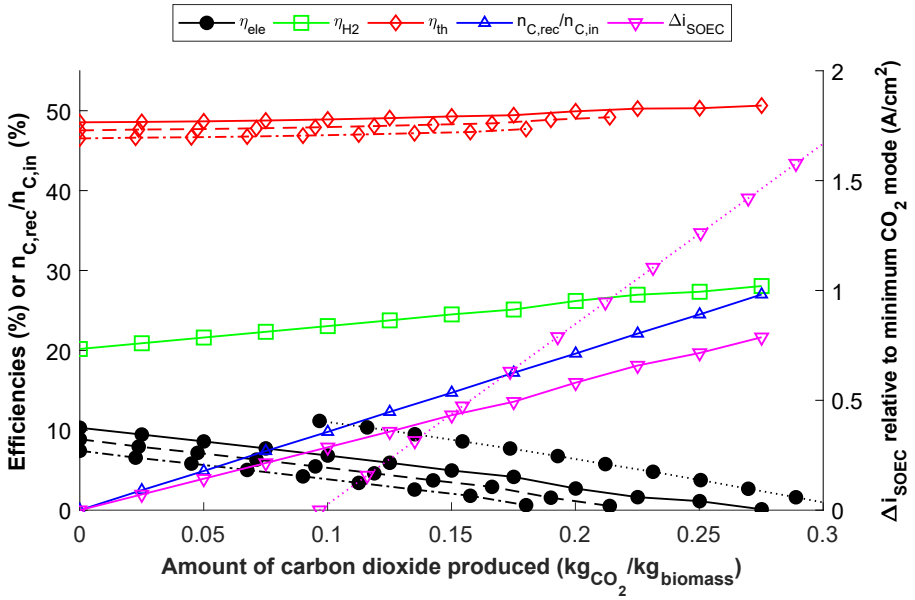

Fig. 10. Variation in efficiencies as a function of the quantity of CO_2 produced by the downdraft gasifier-based system, when no H_2 enrichment is adopted (mode 0). $R_{meth} = 0$ (——), 0.05 (– – –), and 0.1 ((— – —). Data from the DFB-gasifier system at $R_{meth} = 0.4$ are represented by (.....).

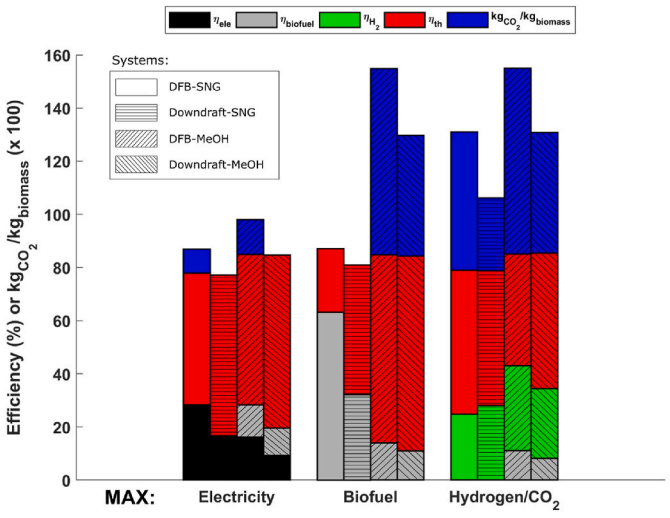

Fig. 11. Comparison of the proposed SNG systems with MeOH-based polygeneration systems [24]. Three scenarios are considered: maximum electricity, SNG/MeOH, or CO_2.

Table 4
Overall energy balance of the two proposed SNG systems and two MeOH-based polygeneration systems [24] at different operating modes.

System	η_{ele}	η_{th}	$\eta_{SNG/MeOH}$	η_{H2}	η_{tot}	kg_{CO2}/kg_{BM}
Maximum electricity production						
DFB-SNG	28.2%	49.6%	0.0%	0.0%	77.9%	0.09
DD-SNG	16.7%	60.5%	0.0%	0.0%	77.1%	0.00
DFB-MeOH	16.1%	56.6%	12.2%	0.0%	84.9%	0.13
DD-MeOH	9.2%	65.1%	10.3%	0.0%	84.6%	0.00
Maximum SNG or MeOH production						
DFB-SNG	0.0%	24.0%	63.1%	0.0%	86.6%	0.00
DD-SNG	0.0%	48.7%	32.2%	0.0%	80.9%	0.00
DFB-MeOH	0.0%	70.8%	14.0%	0.0%	84.8%	0.70
DD-MeOH	0.0%	73.3%	11.0%	0.0%	84.6%	0.45
Maximum H_2 and CO_2 production						
DFB-SNG	0.0%	54.2%	0.0%	24.7%	78.9%	0.52
DD-SNG	0.0%	50.6%	0.0%	28.1%	78.8%	0.28
DFB-MeOH	0.0%	42.0%	11.1%	31.9%	85.0%	0.70
DD-MeOH	0.0%	50.9%	8.2%	26.3%	85.5%	0.45

and also intended for agricultural greenhouses [24]. Three scenarios are shown, where either electricity, biofuel (SNG or MeOH), or CO_2 are maximized, at the expense of the other products. For the latter case, the operating conditions also always coincide with maximum H_2 yield when none of it is recycled into the systems. The difference in maximum electricity and CO_2 output between the SNG and MeOH systems that use the same gasification technique is mainly due to the operating conditions chosen. For instance, more electricity is produced by the SNG configurations since the SOFC is sized at a lower current density $i = 0.5$ A/cm^2 (vs $i = 1.0$ A/cm^2 for MeOH systems), while more CO_2 is generated by the MeOH systems since the SOEC was not operated exothermically above the thermoneutrual voltage. The 28.2% electrical efficiency that can be attained by the DFB-SNG polygeneration system is similar to that of large-scale biomass combined heat and power plants [50], and other studies that combine gasification and SOFCs [32,37].

However, the main advantage of the SNG systems proposed in this paper in the context of safe decentralized operation is clearly the maximum attainable biofuel yield. Due to the milder operating conditions of the chemical reactor and higher syngas conversion fractions, attainable biofuel yields are drastically larger for the SNG systems. For the DFB gasifier-based configurations, maximum $\eta_{biofuel} = 63.1\%$ for SNG, while for MeOH it is only $\eta_{biofuel} = 14.0\%$. The former is comparable with the output of larger single/bi-product SNG systems running on woody biomass [10–13]. For the systems adopting downdraft gasification in Fig. 11, maximum biofuel yield is 32.2% vs 11.0% for SNG and MeOH, respectively.

For the reasons discussed earlier in the text, the efficiencies of the DFB gasifier-based systems prevail over downdraft gasification in both SNG and MeOH systems. This has the potential to outweigh the added complexity and cost of DFB configurations, in addition to the fact that these gasifiers offer the additional benefit of potentially relying on only one RSOC when proper electricity and gas storage medium is available. The RSOC can be operated as a SOFC for a fraction of the time for electricity generation, with air from the ambient atmosphere used in the combustion chamber of the gasifier (shaded region, Fig. 4). Part of the generated electricity is stored, and then injected into the RSOC during its reversed SOEC operating mode where the system produces CO_2. In both of these regimes, heat and SNG are always generated, albeit in variable amounts since H_2 enrichment is only possible in the reverse mode. This subject will be tackled in future transient system simulations where energy storage medium will be incorporated.

4. Conclusion

This paper presents the design and steady-state thermodynamic modelling of two novel small-scale systems capable of producing synthetic natural gas, electricity, heat, and high-purity carbon dioxide from wood chips for agricultural greenhouses. Two gasification techniques are considered, namely steam dual fluidized bed and steam/oxygen-blown downdraft gasifiers. The versatility of reversible solid oxide cells is exploited in various ways, the first being through the efficient and clean generation of electricity and useful heat from syngas. Part of this electricity is then used to synthesize H_2 via steam electrolysis, enriching the methanation reactor and maximizing its SNG yield. The co-produced O_2 is used in the gasification stage, and for oxyfuel combustion, allowing the production of high-purity CO_2 streams for greenhouse atmosphere enrichment.

The overall process efficiency can reach up to 86.6% and 82.5% for the DFB and downdraft gasifier-based configurations, respectively. The share of SNG, electricity, and heat from the total energy output can be readily varied, reaching values comparable with large-scale product-specific systems for the DFB gasifier-based configuration. In this system, η_{SNG} can be varied between 0 and 63.1%, at the expense of η_{ele} that drops from a maximum of 28.2 to 0%, and η_{th} from 49.6 to 24.0%. While for the system adopting the downdraft gasifier, η_{SNG} can be set between 0 and 32.2%, η_{ele} between 0 and 16.7%, and η_{th} between 42.2 and 60.5%. The reduced complexity and cost of downdraft gasifiers come at a cost of lower flexibility and efficiency. Regarding the production of high-purity carbon dioxide, DFB gasifier based-configurations also offer higher capacities of 529 $g_{CO2}/kg_{biomass}$ vs 275 $g_{CO2}/kg_{biomass}$ for the downdraft gasifier-based system. However, in the latter, the drop in electricity output per unit CO_2 produced and the sensitivity of the SOEC current density are much lower.

The proposed systems also offer the possibility of storing excess electrical energy from intermittent energy sources such as photovoltaic cells or wind power. At higher methanation split fractions, the syngas is always deprived of H_2 for optimal SNG yield. Electricity may thus be injected into the SOEC to produce more SNG by enhanced H_2 enrichment. This also produces more O_2 for oxyfuel combustion, which increases the high-purity CO_2 generation capacity, and consequently, the potential carbon negativity of the process. The downdraft gasifier-based configuration offers superior electricity-to-SNG conversion efficiency of 54%, vs 40% for the DFB system, due to the SOEC in the former operating at relatively lower overpotentials.

Following the favorable thermodynamic results reported in this study, the next step would be to assess the economic potential of the novel systems proposed herein. A techno-economic analysis that involves transient system simulations coupled with data acquired from agricultural greenhouses will be used to precisely size the proposed

systems, refine our design choices, and highlight the most profitable operating modes. Following this stage, a laboratory scale demonstrator will be built and rigorously tested with different biomass feedstock. The potential impact goes beyond sustainable agriculture, as new income streams could be created for farmers, transforming them from energy users to energy providers.

CRediT authorship contribution statement

Elie Antar: Conceptualization, Formal analysis, Funding acquisition, Methodology, Software, Validation, Visualization, Writing – original draft, Writing – review & editing. **Etienne Robert:** Conceptualization, Funding acquisition, Methodology, Resources, Supervision, Writing – review & editing.

Declaration of competing interest

The authors declare that they have no known competing financial interests or personal relationships that could have appeared to influence the work reported in this paper.

Data availability

Data will be made available on request.

Acknowledgements

The authors are grateful for the funders of this work: The Trottier Energy Institute (Trottier scholarship and project grant), the Natural Sciences and Engineering Research Council of Canada (NSERC) [PGSD3 - 546588–2020], and the Fonds de Recherche du Québec Nature et technologies (FRQNT) through the Doctoral scholarship (B2X).

Nomenclature

A	Active cell area
$a_{p/r}^{vi}$:	Activity of species i in products (p) or reactants (r)
ASR	Area specific resistance
BM	Biomass
DFB	Dual fluidized bed
DME	Dimethyl ether
ER	Equivalence ratio
F	Faraday's constant
FC	Fixed carbon
FICFB	Fast internally circulating fluidized bed
HHV	Higher heating value
i	Current density
LHV	Lower heating value
$\dot{m}$:	Mass flow rate
M	Feed gas module
MeOH	Methanol
n:	Number of electrons transferred during the electrochemical reaction
$n_{H_2,r}$:	Number of H_2 moles undergoing electrochemical reactions
$n_{C,rec}/n_{C,in}$:	Number of recoverable over input carbon moles
PM	Particulate matter
PSA	Pressure swing adsorption
RSOC:	Reversible solid oxide cell
R_{meth}:	Methanation reactor
S/B	Steam to biomass ratio
S/C	Steam to carbon ratio
SNG	Substitute natural gas
SOEC	Solid oxide electrolysis cell
SOFC	Solid oxide fuel cell
V^o:	Reversible cell voltage at standard conditions
V_{rev}:	Reversible cell voltage
V_{op}:	Operational voltage
VM	Volatile matter
U_f	Fuel utilization factor
U_o	Oxidizer utilization factor
WGS	Water gas shift
η_i:	Efficiency of energy form i = {total, net electrical, thermal, biofuel}
η_{CG}:	Cold gas efficiency of gasifier based on the LHV

References

[1] Yousuf A, Pirozzi D, Sannino F. Fundamentals of lignocellulosic biomass. Academic Press; 2019. https://doi.org/10.1016/B978-0-12-815936-1.00001-0.

[2] Ahamed MS, Guo H, Tanino K. Energy saving techniques for reducing the heating cost of conventional greenhouses. Biosyst Eng 2019. https://doi.org/10.1016/j.biosystemseng.2018.10.017.

[3] Statistics Canada. Report on energy supply and demand in Canada. 2019.

[4] Wang M, Liu C, Xu X, Li Q. Theoretical study of the pyrolysis of vanillin as a model of secondary lignin pyrolysis. Chem Phys Lett 2016;654:41–5. https://doi.org/10.1016/j.cplett.2016.03.058.

[5] Er-rbib H, Bouallou C. Modeling and simulation of CO methanation process for renewable electricity storage. Energy 2014;75:81–8. https://doi.org/10.1016/J.ENERGY.2014.05.115.

[6] Rönsch S, Schneider J, Matthischke S, Schlüter M, Götz M, Lefebvre J, Prabhakaran P, Bajohr S. Review on methanation – from fundamentals to current projects. Fuel 2016;166:276–96. https://doi.org/10.1016/J.FUEL.2015.10.111.

[7] Lange J-P. Methanol synthesis: a short review of technology improvements. Catal Today 2001;64:3–8. https://doi.org/10.1016/S0920-5861(00)00503-4.

[8] Sikarwar VS, Zhao M, Fennell PS, Shah N, Anthony EJ. Progress in biofuel production from gasification. Prog Energy Combust Sci 2017;61:189–248. https://doi.org/10.1016/j.pecs.2017.04.001.

[9] Haro P, Johnsson F, Thunman H. Improved syngas processing for enhanced Bio-SNG production: a techno-economic assessment. Energy 2016;101:380–9. https://doi.org/10.1016/J.ENERGY.2016.02.037.

[10] Tremel A, Matthias G, Hartmut S. Small-scale production of synthetic natural gas by allothermal biomass gasification. Int J Energy Res 2013;37. https://doi.org/10.1002/er.

[11] Gröbl T, Walter H, Haider M. Biomass steam gasification for production of SNG – process design and sensitivity analysis. Appl Energy 2012;97:451–61. https://doi.org/10.1016/J.APENERGY.2012.01.038.

[12] Fendt S, Tremel A, Gaderer M, Spliethoff H. The potential of small-scale SNG production from biomass gasification. Biomass Conv. Bioref. 2012;2:275–83. https://doi.org/10.1007/s13399-012-0037-3.

[13] Rehling B, Hofbauer H, Rauch R, Aichernig C, Hofbauer H, Rauch R, Rehling B, Aichernig C. BioSNG-process simulation and comparison with first results from a 1-MW demonstration plant. Biomass Conv. Bioref. 2011;1:111–9. https://doi.org/10.1007/s13399-011-0013-3.

[14] Rönsch S, Kaltschmitt M. Bio-SNG production-concepts and their assessment. Biomass Convers. Biorefinery. 2012;2:285–96. https://doi.org/10.1007/s13399-012-0048-0.

[15] Wirth S, Markard J. Context matters: how existing sectors and competing technologies affect the prospects of the Swiss Bio-SNG innovation system. Technol Forecast Soc Change 2011;78:635–49. https://doi.org/10.1016/J.TECHFORE.2011.01.001.

[16] Arteaga-Pérez LE, Gómez-Cápiro O, Karelovic A, Jiménez R. A modelling approach to the techno-economics of Biomass-to-SNG/Methanol systems: standalone vs Integrated topologies. Chem. Eng. J. 2016;286:663–78. https://doi.org/10.1016/J.CEJ.2015.11.005.

[17] Sigurjonsson HÆ, Clausen LR. Solution for the future smart energy system: a polygeneration plant based on reversible solid oxide cells and biomass gasification producing either electrofuel or power. Appl Energy 2018;216:323–37. https://doi.org/10.1016/J.APENERGY.2018.02.124.

[18] Gassner M, Maréchal F. Thermo-economic optimisation of the polygeneration of synthetic natural gas (SNG), power and heat from lignocellulosic biomass by gasification and methanation. Energy Environ Sci 2012;5:5768–89. https://doi.org/10.1039/C1EE02867G.

[19] Li Y, Ding Y, Li D, Miao Z. Automatic carbon dioxide enrichment strategies in the greenhouse: a review. Biosyst Eng 2018;171:101–19. https://doi.org/10.1016/J.BIOSYSTEMSENG.2018.04.018.

[20] Dion L-M, Lefsrud M, Orsat V, Cimon C. Biomass gasification and syngas combustion for greenhouse CO2 enrichment. Bioresources 2013;8:1520–38.

[21] Clausen LR, Elmegaard B, Ahrenfeldt J, Henriksen U. Thermodynamic analysis of small-scale dimethyl ether (DME) and methanol plants based on the efficient two-stage gasifier. Energy 2011;36:5805–14. https://doi.org/10.1016/J.ENERGY.2011.08.047.

[22] Jana K, De S. Polygeneration using agricultural waste: thermodynamic and economic feasibility study. Renew Energy 2015;74:648–60. https://doi.org/10.1016/J.RENENE.2014.08.078.

[23] Heyne S, Thunman H, Harvey S. Extending existing combined heat and power plants for synthetic natural gas production. Int J Energy Res 2012;36:670–81. https://doi.org/10.1002/ER.1828.

[24] Antar E, Robert E. Thermodynamic analysis of novel methanol polygeneration systems for greenhouses. Biomass Convers. Biorefinery. 2023;13:8033–46. https://doi.org/10.1007/s13399-021-01678-5.

[25] Hanchate N, Ramani S, Mathpati CS, Dalvi VH. Biomass gasification using dual fluidized bed gasification systems: a review. J Clean Prod 2021;280. https://doi.org/10.1016/j.jclepro.2020.123148.

[26] Clausen LR. Energy efficient thermochemical conversion of very wet biomass to biofuels by integration of steam drying, steam electrolysis and gasification. Energy 2017;125:327–36. https://doi.org/10.1016/J.ENERGY.2017.02.132.

[27] Susastriawan AAP, Saptoadi H. Purnomo, Small-scale downdraft gasifiers for biomass gasification: a review. Renew Sustain Energy Rev 2017;76:989–1003. https://doi.org/10.1016/J.RSER.2017.03.112.

[28] Heidenreich S, Foscolo PU. New concepts in biomass gasification. Prog Energy Combust Sci 2015;46:72–95. https://doi.org/10.1016/j.pecs.2014.06.002.

[29] Zhang R, Brown RC, Suby A, Cummer K. Catalytic destruction of tar in biomass derived producer gas. Energy Convers Manag 2004;45:995–1014. https://doi.org/10.1016/j.enconman.2003.08.016.

[30] Sato K, Fujimoto K. Development of new nickel based catalyst for tar reforming with superior resistance to sulfur poisoning and coking in biomass gasification. Catal Commun 2007;8:1697–701. https://doi.org/10.1016/J.CATCOM.2007.01.028.

[31] Torres W, Pansare SS, Goodwin JG. Hot Gas Removal of Tars, Ammonia, and Hydrogen Sulfide from Biomass Gasification Gas 2007:407–56. https://doi.org/10.1080/01614940701375134. 10.1080/01614940701375134. 49.

[32] Sadegh-Vaziri R, Bäbler MU. Providing sulfur free syngas to a fuel cell system. Energy Proc 2019;159:448–53. https://doi.org/10.1016/J.EGYPRO.2018.12.041.

[33] Baldinelli A, Cinti G, Desideri U, Fantozzi F. Biomass integrated gasifier-fuel cells: experimental investigation on wood syngas tars impact on NiYSZ-anode Solid Oxide Fuel Cells. Energy Convers Manag 2016;128:361–70. https://doi.org/10.1016/J.ENCONMAN.2016.09.048.

[34] Skrzypkiewicz M, Wierzbicki M, Stępień M. Solid Oxide Fuel Cells coupled with a biomass gasification unit. E3S Web Conf 2016;10:1–5. https://doi.org/10.1051/e3sconf/20161000115.

[35] Gadsbøll RØ, Vivar Garcia A, Ahrenfeldt J, Henriksen UB. Solid oxide fuel cell stack coupled with an oxygen-blown TwoStage gasifier using minimal gas cleaning. Renew Energy 2019;139:1255–62. https://doi.org/10.1016/J.RENENE.2019.03.038.

[36] Bao C, Wang Y, Feng D, Jiang Z, Zhang X. Macroscopic modeling of solid oxide fuel cell (SOFC) and model-based control of SOFC and gas turbine hybrid system. Prog Energy Combust Sci 2018;66:83–140. https://doi.org/10.1016/J.PECS.2017.12.002.

[37] Minutillo M, Perna A, Jannelli E, Cigolotti V, Nam SW, Yoon SP, Kwon BW. Coupling of biomass gasification and SOFC – gas turbine hybrid system for small scale cogeneration applications. Energy Proc 2017;105:730–7. https://doi.org/10.1016/J.EGYPRO.2017.03.383.

[38] Di Salvo M, Wei M. Synthesis of natural gas from thermochemical and power-to-gas pathways for industrial sector decarbonization in California. Energy 2019;182:1250–64. https://doi.org/10.1016/J.ENERGY.2019.04.212.

[39] Heyne S. Bio-SNG from thermal gasification-process synthesis, integration and performance. Chalmers University of Technology; 2013. http://publications.lib.chalmers.se/records/fulltext/175377/175377.pdf. [Accessed 15 August 2019].

[40] Zhu L, He Y, Li L, Lv L, He J. Thermodynamic assessment of SNG and power polygeneration with the goal of zero CO2 emission. Energy 2018;149:34–46. https://doi.org/10.1016/J.ENERGY.2018.02.032.

[41] Damartzis T, Michailos S, Zabaniotou A. Energetic assessment of a combined heat and power integrated biomass gasification–internal combustion engine system by using Aspen Plus®, Fuel Process. Technol 2012;95:37–44. https://doi.org/10.1016/J.FUPROC.2011.11.010.

[42] Doherty W, Reynolds A, Kennedy D. Aspen plus simulation of biomass gasification in a steam blown dual fluidised bed. Book Chapter: Materials and processes for energy: communicating current research and technological developments. Formatex Research Centre; 2013.

[43] Han J, Liang Y, Hu J, Qin L, Street J, Lu Y, Yu F. Modeling downdraft biomass gasification process by restricting chemical reaction equilibrium with Aspen Plus. Energy Convers Manag 2017:641–8. https://doi.org/10.1016/j.enconman.2017.10.030.

[44] Karellas S, Panopoulos KD, Panousis G, Rigas A, Karl J, Kakaras E. An evaluation of Substitute natural gas production from different coal gasification processes based on modeling. Energy 2012;45:183–94. https://doi.org/10.1016/J.ENERGY.2012.03.075.

[45] Butera G, Jensen SH, Clausen LR. A novel system for large-scale storage of electricity as synthetic natural gas using reversible pressurized solid oxide cells. Energy 2019;166:738–54. https://doi.org/10.1016/J.ENERGY.2018.10.079.

[46] O'Hayre R, Cha S-W, Colella W, Prinz FB. Fuel cell fundamentals. John Wiley & Sons, Inc; 2016. https://doi.org/10.1002/9781119191766.

[47] Mesfun S, Lundgren J, Toffolo A, Lindbergh G, Lagergren C, Engvall K. Integration of an electrolysis unit for producer gas conditioning in a bio-synthetic natural gas plant. J. Energy Resour. Technol. Trans. ASME. 2019;141:1–12. https://doi.org/10.1115/1.4040942.

[48] Clausen LR, Butera G, Jensen SH. High efficiency SNG production from biomass and electricity by integrating gasification with pressurized solid oxide electrolysis cells. Energy 2019;172:1117–31. https://doi.org/10.1016/J.ENERGY.2019.02.039.

[49] Gassner M, Maréchal F. Thermo-economic optimisation of the integration of electrolysis in synthetic natural gas production from wood. Energy 2008;33:189–98. https://doi.org/10.1016/j.energy.2007.09.010.

[50] Islas J, Manzini F, Masera O, Vargas V. Solid biomass to heat and power. In: Role bioenergy emerg. Bioeconomy resour. Technol. Sustain. Policy. Academic Press; 2019. p. 145–77. https://doi.org/10.1016/B978-0-12-813056-8.00004-2.